Available online at www.sciencedirect.com
SCIENCE DIRECT
Journal of Solid State Chemistry 179 (2006) 866–872
JOURNAL OF SOLID STATE CHEMISTRY
www.elsevier.com/locate/jssc

Synthesis and characterization of three-dimensionally ordered macroporous ternary oxide

S. Madhavi*, C. Ferraris, Tim White

School of Materials Science and Engineering, Nanyang Technological University, Block N4.1-B4-10, 50 Nanyang Avenue, Singapore 639798, Singapore

Received 21 September 2005; received in revised form 30 November 2005; accepted 9 December 2005
Available online 20 January 2006

Abstract

A three-dimensionally ordered macroporous (3DOM) ternary oxide, $CsAlTiO_4$, with a framework related to 'stuffed-tridymite' has been synthesized at temperatures 500–700 °C using a sol–gel precursor solution and templating with polystyrene spheres. The 3DOM material displayed pore diameters of 0.5–0.8 μm with the walls composed of anhedral and acicular $CsAlTiO_4$ crystals whose dimensions ranged from 16 to 25 nm. Microanalysis confirmed near-stoichiometric proportions (1:1:1) of Cs, Al and Ti. The effect of sintering temperature on the macroporous structure and on the $CsAlTiO_4$ walls was studied. As the sintering temperature increased from 500 to 600 °C the unit cell parameters varied through dilation (*a* and *b*) and contraction (*c*-axis), followed by a reversal of these trends from 700 to 900 °C. This behaviour in non-equilibrated $CsAlTiO_4$ can be attributed to distortion of the (Al, Ti)O_4 tetrahedral framework, however at the highest temperature the cell constants stabilized close to those reported for single crystal $CsAlTiO_4$. X-ray amorphous content was significant in all materials varying from 73 wt% after 500°C and reducing to 44 wt% at 900 °C.

Keywords: Macroporous; $CsAlTiO_4$; Stuffed-tridymite; Colloidal-crystal templating; Rietveld analysis

1. Introduction

Three-dimensionally ordered macroporous (3DOM) materials [1–10], synthesized from self-assembled silica or polymer sphere templates, are of considerable interest because of their potential application as photonic interconnects [11,12], membranes [13,14], catalysts [15,16], and biomaterials [17–19]. Using a two-stage process, the interstices of a face-centred cubic (fcc) close-packed array of spheres can be impregnated with a fluid precursor that subsequently solidifies, followed by sphere removal to obtain the 3DOM replica. Through altering the precursor chemistry and/or the infiltration process, a variety of macroporous materials ranging from metals to ceramics and polymers can be prepared [1–10]. The most commonly reported 3DOM ceramics, viz., TiO_2 [1,7,20–22], SiO_2 [2,7,9], Al_2O_3 [1,20] and ZrO_2 [1,15,20,23] are usually synthesized from organic precursor solutions. Other oxides like V_2O_5 [24,25], SnO_2 [25], NiO [26], ZnO [26], Fe_2O_3 [3,26], Co_3O_4 [26], Cr_2O_3 [26], Mn_2O_3 [26] and rare-earth oxides (CeO_2, La_2O_3) [27] have been prepared by precipitation of their respective metal salts (acetates or oxalates). The synthesis of simple oxides with 3DOM architecture is relatively direct, as compared to binary oxides, which require stable precursor solutions prepared from a mixture of metal alkoxides and salts. Recently, the synthesis of macroporous binary oxides such as $BaTiO_3$ [28,29], $PbTiO_3$ [30], $LiAlO_2$ [31], $LiNiO_2$ [25], metal-doped binary oxides including $PbZr_{0.2}Ti_{0.8}O_3$ [30,32], and $La_{0.7}Ca_{0.3}MnO_3$ [32,33] have been reported. However, 3DOM ternary metal oxide synthesis involving near equimolar quantities of three metals in the oxide lattice is less straightforward as homogeneous precipitation/gelation at near atomic scale throughout the impregnated volume is essential and to our knowledge has not been reported. Many of the technologically important ecomaterials used in advanced applications contain three or more metals in a specific ratio. Hence the ability to synthesize chemically complex and functional 3DOM ceramics is of particular

*Corresponding author. Fax: +65 6790 9081.
E-mail address: madhavi@ntu.edu.sg (S. Madhavi).

0022-4596/$ - see front matter © 2005 Elsevier Inc. All rights reserved.
doi:10.1016/j.jssc.2005.12.010

relevance for their application as ecomaterials, if the intrinsically high porosity, low density and large effective surface area are to be exploited. We report the synthesis and characterization of one such ecomaterial, microporous $CsAlTiO_4$. Our interest in such systems is two-fold and focuses on (i) the development of methods to synthesize 3DOM structures containing ternary metal oxides, and (ii) potential technological applications of bimodal porous structures, viz., a macroporous network structure comprising of microporous walls. Such macro-micro porous materials provide bimodal pore systems, which combine the benefits of each pore size regime.

Previously, Holland et al. [34], using hydrothermal methods prepared zeolitic silicates in macroporous form, but this work was not extended to mixed ternary cation materials. $CsAlTiO_4$ [35–37] belongs to a general class of $ABCO_4$ (A = K, Rb, Cs; B = Al, C = Si, Ti) compounds that are similar to the 'stuffed tridymites' but differ in the orientation of the corner-connected (B, C)O_4 units such that some 6-membered tetrahedral rings are converted to 4- and 8-membered rings (Fig. 1) [35–37]. Moreover, the corner-connectivity of the tetrahedra allows co-operative rotation and adjustment of A–O bond lengths to best accommodate the large cation. In $CsAlTiO_4$, the framework cavities approach full expansion (i.e., (Al, Ti)–O–(Al, Ti) bond angles of 180°) for cesium incorporation, but collapse for smaller potassium and rubidium analogues. It is interesting to note that this is one of the few titanium (IV) compounds in which TiO_4 tetrahedra are present (Fig. 1c). The primary objective of the present study was to establish the optimized conditions to synthesize 3DOM ternary microporous $CsAlTiO_4$ ecomaterial. The evolution of crystallinity and the amorphous material content in the samples was of particular interest and was investigated by Rietveld analysis of powder X-ray diffraction (XRD) data, the interpretation of which was validated using results gathered by analytical high-resolution transmission electron microscopy (ATEM) that allowed direct monitoring of macropore evolution as a function of sintering temperature and time.

2. Experimental procedures

2.1. Macroporous material synthesis

Monodispersed polystyrene latex microsphere suspensions of mean diameter of 1.0 μm and a size distribution of ⩽3% from Duke Scientific Corporation (USA) were used to create templates. $CsAlTiO_4$ was prepared from cesium carbonate (Cs_2CO_3, Merck, 99.90%), titanium butoxide ($Ti(C_4H_9O)_4$, Aldrich), aluminium sec-butoxide ($Al[O(CH_3)CHC_2H_5]_3$, Alfa), glacial acetic acid (Fischer), absolute ethanol (Merck), and distilled water (MilliQ).

The latex microsphere suspension was used as received. About 1–1.5 mL of the suspension was loaded into centrifuge tubes and spun for 48 h at 900 rpm to obtain well-ordered fcc polymer templates. To prevent disturbance by the precursor solution the spheres were fused by heating to 100–150 °C for 15–30 min. The infiltration solution was prepared in three stages: (i) 1 mmol cesium carbonate (Cs_2CO_3) was dissolved in 1–2 mL of glacial acetic acid with vigorous stirring; (ii) 2 mmol titanium butoxide ($Ti(C_4H_9O)_4$) and 2 mmol aluminium sec-butoxide ($Al[O(CH_3)CHC_2H_5]_3$) was diluted in absolute ethanol with a volume ratio of alkoxide to ethanol = 1:15; (iii) these solutions were mixed under vigorous stirring, with the concentration and viscosity of the precursor adjusted by introducing small aliquots of glacial acetic acid

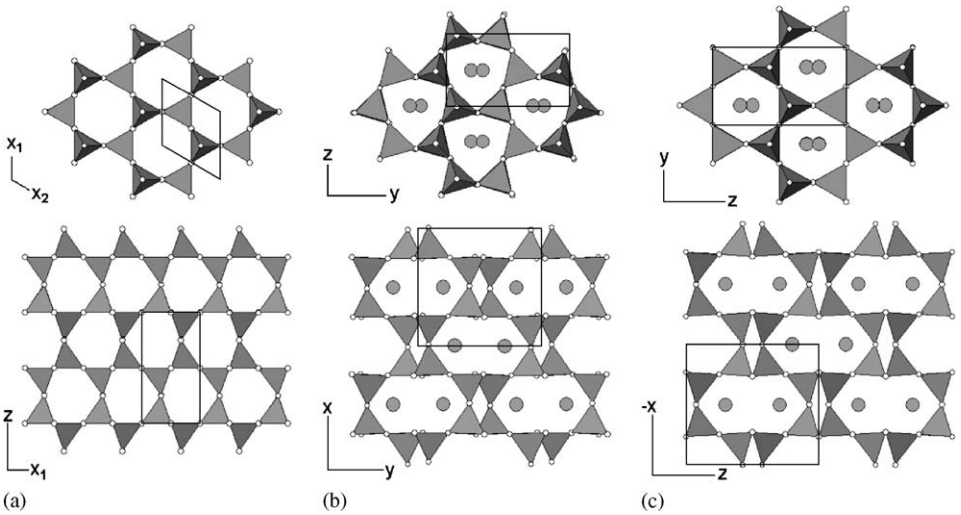

Fig. 1. Structure drawings of tetrahedral framework structures. (a) Ideal tridymite ($P6_3/mmc$) projected along both [001] (upper) and [100] (lower). The vertex up (U) and vertex down (D) orientation of tetrahedra around the 6-membered tetrahedral ring along the hexagonal axis is …U(DUDUDU)D… and all rings are constructed from 6 tetrahedra. (b) In $RbAlSiO_4$ the symmetry is reduced to orthorhombic $Pna2_1$. The tetrahedral orientation along the pseudo-hexagonal projection is …U(DDDUUU)D… leading to a mixture of 4-, 6- and 8-membered ring cavities. In addition, the tetrahedra are tilted to partially collapse the larger cavities in a manner that satisfies Rb–O bond length requirements. (c) $CsAlTiO_4$ (*Imma*) adopts the same tetrahedral topology as $RbAlSiO_4$, but as Cs^+ is larger than Rb^+, the large cavities are almost fully expanded and tetrahedral tilting is much reduced.

(to ensure complete dissolution of $CsCO_3$) and/or ethanol (to delay premature hydrolysis). The final solution was clear. The polystyrene templates were soaked in the admixed solution for 15–30 min, allowing sufficient time for impregnation by capillary action, with the excess solution removed by vacuum filtration. The infiltered templates were dried in a vacuum dessicator for 24 h to enhance the liquid to solid transformation in the walls. Repeated infiltration and gelation steps were carried out (3–5 times) to ensure complete filling of the voids. These composites were sintered in a tube furnace under flowing oxygen at 400 °C for 3 h obtained at a heating rate of 1 °C/min to combust the majority of the polymer. This was immediately followed by calcination at 500–900 °C for 1 h (heating rate: 2 °C/min) to obtain 3DOM $CsAlTiO_4$. Cloudy precursor solutions resulted in the formation of a Ti/Al oxide layer on the template surface that prevented further infiltration of the voids and incomplete sphere burnout. Air sintering invariably lead to partial oxidation of the polymer spheres.

2.2. Characterization techniques

Secondary electron images (SEI) were collected using a JEOL JSM-5310LV scanning microscope operated at 15 or 20 keV to control specimen charging. The samples were coated with a thin layer of gold using an SPI Supplies (USA) sputter coater and placed on conductive carbon tape adhered to an aluminium sample holder. For powder XRD the macroporous powders were dispersed using ethanol on a non-diffracting silicon-wafer specimen holder fitted to a Siemens D5005 diffractometer. Patterns were collected using Cu$K\alpha$ radiation using step-scanning in the 2θ range 10–80° at intervals of 0.02°, and with a stepping time of 14 s. The total collection time per pattern was 13.6 h. Quantitative phase analysis was conducted using the fundamental parameter Rietveld procedure as implemented in TOPAS R (version 2.1) [38]. The crystallographic model was that reported for $CsAlTiO_4$ structure by Gatehouse [36]. For each refinement, the background parameter, scale factor, cell parameter, zero point correction and sample displacement were refined, however the atom positions, site occupancy factors and isotropic thermal parameters were not. Diffraction data were taken for each sample batch with and without a standard alumina spike (20 wt% NIST SRM 676) [39] to determine in absolute terms the crystalline and amorphous content [40–47].

Transmission, scanning and analytical electron microscopy (TEM, STEM and ATEM) were performed at 300 kV using a JEOL JEM 3010 equipped with low-background double-tilt holder, LaB_6 cathode, Gatan Imaging Filter system (GIF), LINK ISIS EDS X-ray microanalysis and a backscattered electron-imaging device (BEI) coupled with STEM. Field-limiting apertures used for selected area electron diffraction (SAED) were 5, 20, and 60 μm in diameter. High-resolution images were collected using a high contrast objective aperture of 20 μm, corresponding to a nominal point-to-point resolution of 0.19 nm. ATEM investigations were performed in

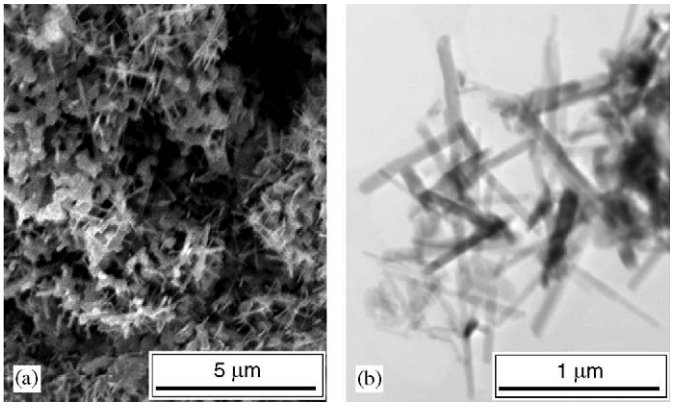

Fig. 3. (a) Secondary electron micrograph and (b) bright field transmission electron micrograph showing growth of acicular $CsAlTiO_4$ crystals and collapse of 3DOM structure.

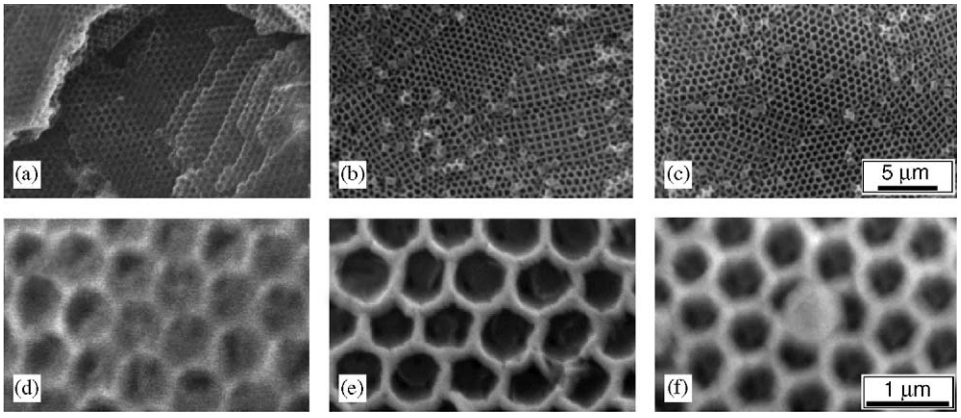

Fig. 2. Secondary electron images showing the macroporous domain size after sintering at (a) 500 °C, (b) 600 °C and (c) 700 °C. At higher magnification the material treated at (d) 500 °C exhibited regions of poor contrast tentatively attributed to incomplete template removal, while at (e) 600 °C clear images were obtained. Firing at (f) 700 °C reduced pore diameter from 0.8 to 0.5 μm due to crystallization and shrinkage.

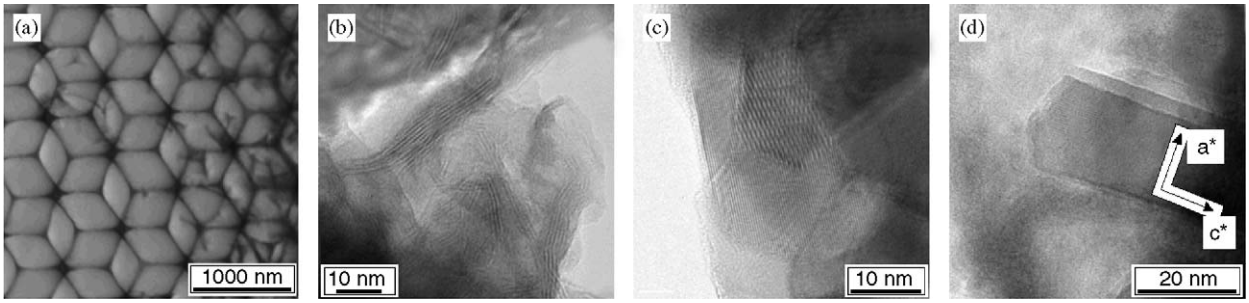

Fig. 4. (a) Bright field transmission electron micrograph of macroporous $CsAlTiO_4$ prepared at 700 °C emphasising the fcc arrangement of voids. (b) Lattice image of 500 °C macropore wall showing serpentine structure. (c) At 600 °C well-defined euhedral crystals are developed and the lattice periodicity is regular. (d) Development of acicular crystals is well-established after firing at 700 °C.

TEM-EDS mode, with live counting time of 50 s and a nominally beam diameter of 25 nm. Recalculation and normalization of the ATEM analyses were performed assuming the thin-film approximation, using experimental calibrations from silicate standards, leading to compositions based upon 4 oxygen atoms per formula unit (a.p.f.u.) for the $CsAlTiO_4$ synthetic compounds. TEM specimens were prepared by gently crushing the macroporous powder under acetone in an agate mortar and pestle, with several drops of the suspension deposited on a copper grid coated with a holey carbon film as a support.

3. Results and discussion

3.1. Macroporous structure

To investigate the effect of temperature on the macroscopic structure and wall crystallinity, samples were heated at different calcination temperatures (500–900 °C) after the removal of polymer spheres. Close-packed void domains of the order of 1000 μm^3 were preserved for samples crystallized at 500, 600 and 700 °C (Fig. 2a–c). In all these samples, the porous structure extended throughout the 3DOM structure indicating uniform infiltration and crystallization. A representative figure of the sample obtained at 500 °C is shown (Fig. 2a). The SEM images of the samples obtained at 600 and 700 °C were similar (Fig. 2b, c) however, the sample fired at 500 °C displayed poorer SEI contrast (Fig. 2d) suggestive of incomplete template oxidation. The pore diameter in samples calcined at 500 and 600 °C ranged from 0.7–0.8 μm which corre-

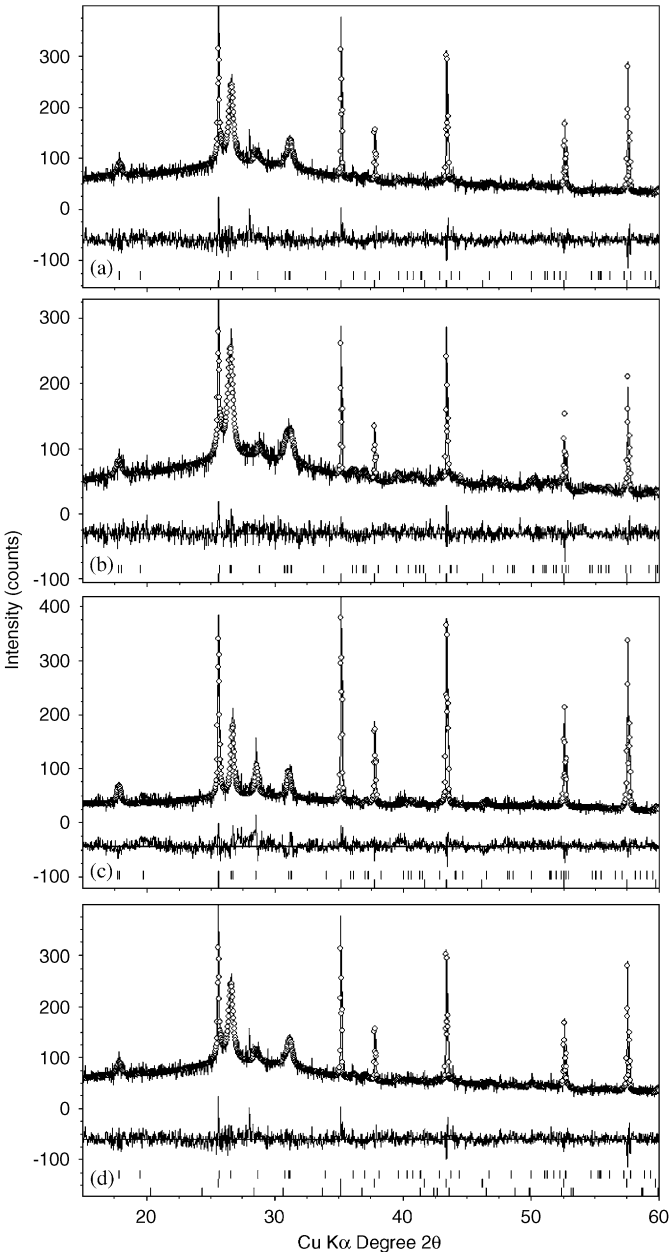

Fig. 5. X-ray diffraction profiles of macroporous $CsAlTiO_4$ synthesized at (a) 500 °C, (b) 600 °C, (c) 700 °C and (d) 900 °C. Experimental data are shown as circles overlaying a simulated pattern (continuous line). The lower trace is the difference between the calculated and experimental intensities. For each trace the Bragg markers from top to bottom are $CsAlTiO_4$, alumina (as an internal standard), and in the case of (d) only, rutile.

sponds to a 20% shrinkage (Fig. 2d–e), a result consistent with earlier 3DOM synthesis employing polymer spheres [1,20,48]. The wall thickness increases significantly at higher temperatures (700 °C) due to the enhanced crystal growth taking place in the nanocrystalline walls of the pore, thus reducing the pore diameter to 0.5–0.6 μm (Fig. 2f). Calcining at 900 °C resulted in the disruption of the macropores due to the formation of large acicular $CsAlTiO_4$ crystals (1–2 μm in length) that exceeded the pore dimensions (Fig. 3). Similarly, sintering at 700 °C for a longer duration (6 h) to improve the crystallinity also resulted in the loss of macroporosity. Therefore, excessive sintering should be avoided to preserve the 3DOM framework.

When examined by bright-field TEM the samples synthesized at 500, 600 and 700 °C showed motifs characteristic of the [111] projection of a fcc inverse opaline structure (Fig. 4a). The thickness of the macroporous walls was about 10–20 nm. Quantitative ATEM were consistent with the expected atomic ratio of cations Cs:Al:Ti = 1:1:1 for $CsAlTiO_4$. Crystal perfection progressively improved as the sintering temperature was raised. Lattice images of the 500 °C material revealed serpentine features in the walls consistent with lattice mismatch that may be arising from partial ordering of metals and/or loss of intercalated organic precursors (Fig. 4b). This relatively poor order was also reflected in SAED patterns that showed weak intensity. Raising the sintering temperature to 600 °C gave rise to faceted euhedral crystals (Fig. 4c), however at 700 °C crystal growth lead to acicular crystals 60 × 25 nm in dimension (Fig. 4d). As already noted above samples synthesized at 900 °C showed large $CsAlTiO_4$ needles, however these did not self-assemble to preserve the macroporous architecture, as has been observed previously for 3DOM hydroxyapatite [47].

3.2. Crystal structure

XRD confirmed that $CsAlTiO_4$ was the dominant crystalline phase present in the macroporous walls for all samples, together with trace (<1 wt%) cesium titanate ($Cs_{0.6}Ti_{1.84}O_4$) [49] in material synthesized at 500 and 600 °C (Fig. 5a–c). As this phase was absent in the samples prepared at 700 °C or higher it is suspected to be a low-temperature intermediate phase. The formation of minor traces (< 2%) of TiO_2 (rutile) at 900 °C (Fig. 5d) is noted and is consistent with observations by Peres et al. [50] during the sol–gel synthesis of $CsAlTiO_4$ powders.

The lattice parameters and crystal sizes of $CsAlTiO_4$ synthesized at various temperatures are listed in Table 1 and compared with those of single crystal $CsAlTiO_4$ reported by Gatehouse [36]. After firing at 900 °C the cell constants were close to those reported for equilibrated single crystal material, however the approach to equilibrium was circuitous. While the lattice constants for *a* and *b* initially dilated, and *c* contracted, in passing from 500 to

Table 1
Refined cell parameters of macroporous $CsAlTiO_4$

Sintering temperature (°C)	Lattice parameters[a] (Å)			Cell volume (Å^3)	Crystallite size (nm)	R_b[b] (%)	X-ray amorphous content (%)
	a	*b*	*c*				
500	9.098(5)	5.730(4)	9.952(7)	519	16	4.4	73
600	9.128(4)	5.771(4)	9.874(5)	520	22	4.3	72
700	9.004(7)	5.718(7)	9.999(5)	515	25	7.4	54
900	9.006(6)	5.740(5)	9.958(8)	515	80	5.7	44
$CsAlTiO_4$[36]	8.978(4)	5.740(1)	9.969(2)	514	—	—	—

[a]esd shown in parentheses.
[b]Bragg *R*-factor.

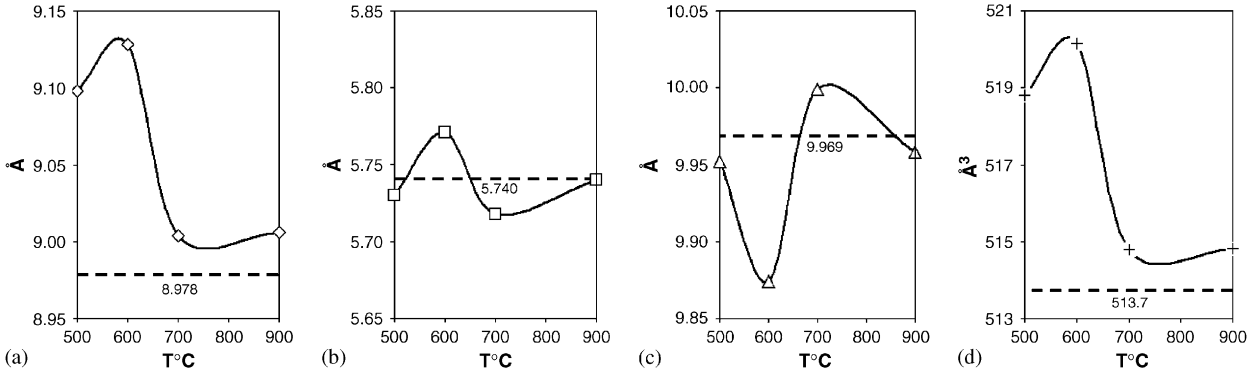

Fig. 6. The variation in (a) *a*-cell edge, (b) *b*-cell edge, (c) *c*-cell edge and (d) unit cell volume for $CsAlTiO_4$ as a function of annealing temperature. The dashed line shows the cell constants for equilibrated single-crystal material as reported by Gatehouse [36].

600 °C, this trend reversed from 700 to 900 °C (Fig. 6a–c). Overall the unit cell volume decreased and stabilized at 514.8(8) Å^3 at temperatures >700 °C. The relatively complex evolution of the structure is related to the framework nature of $CsAlTiO_4$. As a three-dimensional tunnel structure, $CsAlTiO_4$ can be regarded as zeolite-like as the Cs is ion exchangeable and non-stoichiometry could be accommodated through introducing counter-ions in the Al–Ti framework. Channels of two types occur; those consisting of eight tetrahedral with a width of 4.16 Å along [010] and the second consisting of six tetrahedral and a diameter of 5.76 Å. In both cases, these channels are large enough to allow relatively free movement of cesium via ion exchange. Gatehouse [36] reported the anisotropic thermal parameters for a single crystal and these are shown as thermal ellipsoids in Fig. 7. It is apparent that the material is exceedingly flexible (consider the highly elongated ellipsoid for O(3)) and during crystallization tetrahedral tilting will adjust locally to accommodate the contents of the large cavities. As the tetrahedra are essentially rigid bodies, the total circumference of the large channel must remain invariant. Therefore, in the [010] projection any increase in the *a*-cell edge will be matched by a decrease in the *c*-parameter. The X-ray data collected in this investigation was inadequate to refine atomic positions so as to examine this point in greater detail.

The XRD peaks were broadened at lower sintering temperatures in a manner consistent with the TEM observation of finely divided crystals, but sharpened at 900 °C with the appearance of larger crystals. The average crystal size from Rietveld refinement increased from 16 to 80 nm with higher temperatures (500–900 °C) and are comparable to the microscopic observations, taking into account the averaging of size and shape inherent in the Rietveld determination (Table 1). The X-ray amorphous content present in these materials was inversely proportional to sintering temperature and decreased from 73% at 500 °C to 44% at 900 °C. Intergranular, non-diffracting material was also imaged by TEM. The short sintering duration employed in this work is essential to preserve the macroporous network thus compromising wall crystallinity. The contribution of the residual carbon from the polymer template is unknown, but as the sintering was carried out in oxygen, this is expected to be minimal. As a general observation, it is noted that the relatively lower sintering temperature and shorter duration employed in 3DOM material synthesis is likely to result in substantial amorphous content. Since many of the mono and binary 3DOM material systems are being considered for various advanced applications, we believe it imperative to determine amorphous content to better understand their physical properties.

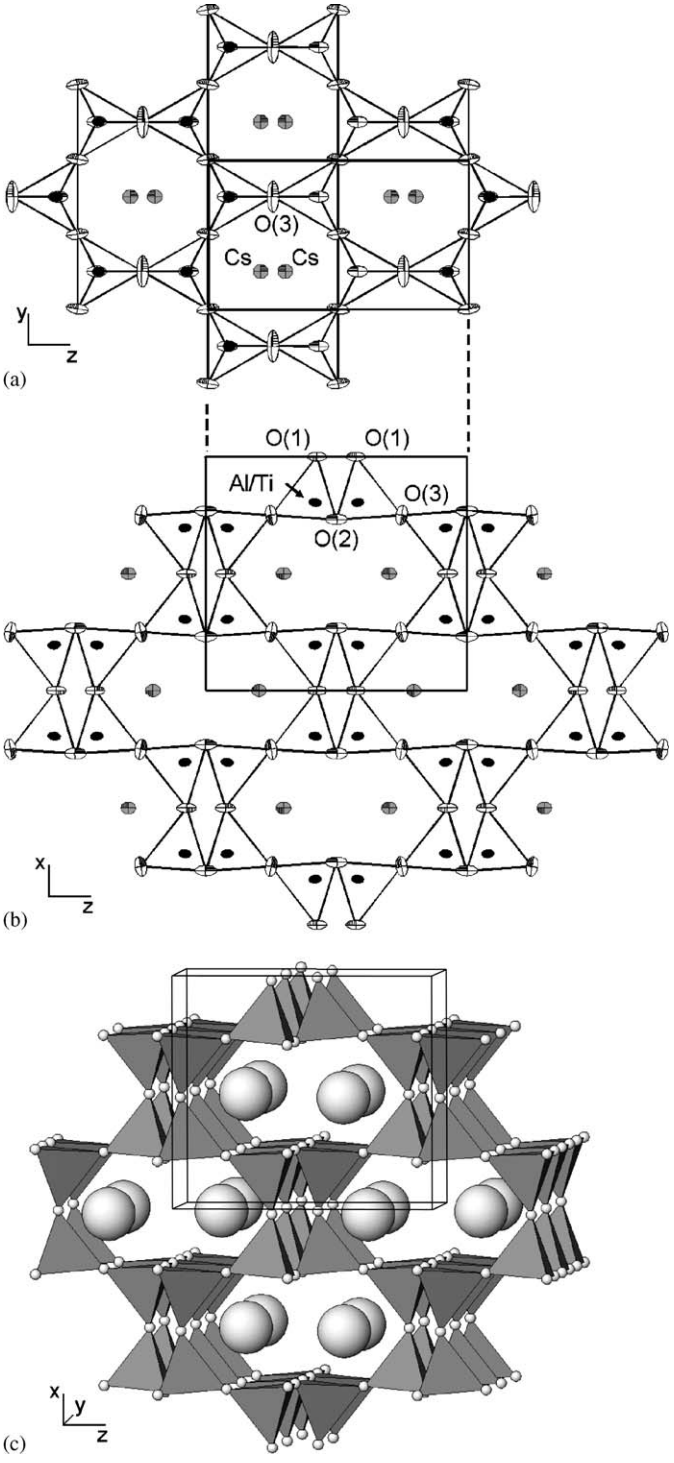

Fig. 7. The structure of $CsAlTiO_4$ as determined by Gatehouse [36] viewed in (a) [100], (b) [010] projections emphasising the thermal ellipsoids and (c) three-dimensional view. The vibration for the oxygen atoms is large and reflects the inherent flexibility of the corner-connected tetrahedral network. This flexibility allows considerable variation in cell-constants as observed in poorly equilibrated material.

4. Summary

Three-dimensionally ordered macroporous (3DOM) networks with ternary metal oxide, $CsAlTiO_4$, microporous walls have been synthesized. The pore size, which varied between 0.5 and 0.8 μm for sintering temperatures 500–700 °C, collapsed at 900 °C due to the formation of acicular $CsAlTiO_4$ crystals. While the sole crystalline phase

was $CsAlTiO_4$, X-ray amorphous content ranged from 44% to 73% due to the short annealing times and low-temperatures employed. Longer sintering time (6 h) resulted in excessive grain growth and the collapse of the macroporous structure. These results show that the optimal condition to retain the macroporous structure and to obtain crystalline $CsAlTiO_4$ walls is 700 °C for 1 h.

Acknowledgments

The authors thank Dr. R.S. Roth for locating a copy of his early report concerning $CsAlTiO_4$ synthesis. This work was supported through the Agency for Science, Technology and Research, Singapore (A*STAR Grant 012 105 0123; A*STAR Grant 032 101 0023).

References

[1] B.T. Holland, C.F. Blanford, A. Stein, Science 281 (1998) 538–540.
[2] O.D. Velev, E.W. Kaler, Adv. Mater. 12 (2000) 531–534.
[3] C.F. Blanford, H. Yan, R.C. Schroden, M. Al-Daous, A. Stein, Adv. Mater. 13 (2001) 401–407.
[4] P.V. Braun, P. Wiltzius, Curr. Opin. Colloid Interface Sci. 7 (2002) 116–123.
[5] F. Meseguer, A. Blanco, H. Miguez, F.G. Santamaria, M. Ibisate, C. Lopez, Colloids Surf. A: Physicochem. Eng. Aspects 202 (2002) 281–290.
[6] Y. Xia, B. Gates, Y. Yin, Y. Lu, Adv. Mater. 12 (2000) 693–713.
[7] A. Stein, Micropor. Mesopor. Mater. 44/45 (2001) 227–239.
[8] A. Stein, R.C. Schroden, Curr. Opin. Solid State Mater. Sci. 5 (2001) 553–564.
[9] O.D. Velev, A.M. Lenhoff, Curr. Opin. Colloids Interface Sci. 5 (2000) 56–63.
[10] A.K. Srivastava, S. Madhavi, T.J. White, R.V. Ramanujan, J. Mater. Chem. 15 (2005) 4424–4428.
[11] J.E.G.J. Wijnhoven, W.L. Vos, Science 281 (1998) 802–804.
[12] P.V. Braun, P. Wiltzius, Nature 402 (1999) 603–604.
[13] B. Gates, Y. Yin, Y. Xia, Chem. Mater. 11 (1999) 2827–2836.
[14] S.H. Park, Y. Xia, Adv. Mater. 10 (1998) 1045–1048.
[15] M.A. Al-Daous, A. Stein, Chem. Mater. 15 (2003) 2638–2645.
[16] M.A. Carreon, V.V. Guliants, Chem. Mater. 14 (2002) 2670–2675.
[17] H. Yan, K. Zhang, C.F. Blanford, L.F. Francis, A. Stein, Chem. Mater. 13 (2001) 1374–1382.
[18] B.J. Melde, A. Stein, Chem. Mater. 14 (2002) 3326–3331.
[19] K. Zhang, H. Yan, D.C. Bell, A. Stein, L.F. Francis, J. Biomed. Mater. Res. 66A (2003) 860–869.
[20] B.T. Holland, C.F. Blanford, T. Do, A. Stein, Chem. Mater. 11 (1999) 795–805.
[21] M. Lanata, M. Cherchi, A. Zappettini, S.M. Pietralunga, M. Martinelli, Opt. Mater. 17 (2001) 11–14.
[22] M.E. Turner, T.J. Trentler, V.L. Colvin, Adv. Mater. 13 (2001) 180–183.
[23] S. Ramesh, E. Sominska, A. Gedanken, Ultrasonics Sonochem. 9 (2002) 61–64.
[24] J.S. Sakamoto, B. Dunn, J. Mater. Chem. 12 (2002) 2859–2861.
[25] H. Yan, S. Sokolov, J.C. Lytle, A. Stein, F. Zhang, W.H. Smyrl, J. Electrochem. Soc. 150 (2003) A1102–A1107.
[26] H. Yan, C.F. Blanford, J.C. Lytle, C.B. Carter, W.H. Smyrl, A. Stein, Chem. Mater. 13 (2001) 4314–4321.
[27] Q.Z. Wu, Y. Shen, J.F. Liao, Y.G. Li, Mater. Lett. 58 (2004) 2688–2691.
[28] Z. Lei, J. Li, Y. Zhang, S. Lu, J. Mater. Chem. 10 (2000) 2629–2631.
[29] P. Harkins, D. Eustace, J. Gallagher, D.W. McComb, J. Mater. Chem. 12 (2002) 1247–1249.
[30] G. Gundiah, C.N.R. Rao, Solid State Sci. 2 (2000) 877–882.
[31] S. Sokolov, A. Stein, Mater. Lett. 57 (2003) 3593–3597.
[32] Y.N. Kim, E.O. Chi, J.C. Kim, E.K. Lee, N.H. Hur, Solid State Commun. 128 (2003) 339–343.
[33] E.O. Chi, Y.N. Kim, J.C. Kim, N.H. Hur, Chem. Mater. 15 (2003) 1929–1931.
[34] B.T. Holland, L. Abrams, A. Stein, J. Am. Chem. Soc. 121 (1999) 4308–4309.
[35] R.S. Roth, W.S. Brower, M. Austin, M. Koob, Phase stability, National Measurement Laboratory Office of Measurements for Nuclear Technology Annual Report, NBSIR 81-2441, 1981, pp. 41–49.
[36] B.M. Gatehouse, Acta Crystallogr. C 45 (1989) 1674–1677.
[37] H.K. Muller-Buschbaum, J. Alloys Compd. 349 (2003) 49–104.
[38] R.W. Cheary, A. Coelho, J. Appl. Cryst. 25 (1992) 109–121.
[39] W.P. Reed, Certificate SRM 676, National Institute of Standards and Technology (NIST), Gaithersburg, MD 20899, 1992.
[40] A.G. De La Torre, S. Bruque, M.A.G. Aranda, J. Appl. Crystallogr. 34 (2001) 196–202.
[41] R.S. Winburn, Proceedings of the 51st Annual Conference on Application of X-ray Analysis, Advances in X-ray Analysis, USA, vol. 46, 2002, pp. 210–219.
[42] F. Guirado, S. Gali, S. Chinchon, Cement Concrete Res. 30 (2000) 1023–1029.
[43] P.S. Whitfield, L.D. Mitchell, J. Mater. Sci. 38 (2003) 4415–4421.
[44] X. Orlhac, C. Fillet, P. Deniard, A.M. Dulac, R. Brec, J. Appl. Crystallogr. 34 (2001) 114–118.
[45] T.E. Gills, Certificate SRM 656, National Institute of Standards and Technology (NIST), Gaithersburg, 1995.
[46] R. Kumar, P. Cheang, K.A. Khor, Acta Mater. 52 (2004) 1171–1181.
[47] S. Madhavi, C. Ferraris, T.J. White, J. Solid State Chem. 178 (2005) 2838–2845.
[48] H. Yan, C.F. Blanford, B.T. Holland, W.H. Smyrl, A. Stein, Chem. Mater. 12 (2000) 1134–1141.
[49] I.E. Grey, C. Li, I.C. Madsen, J.A. Watts, J Solid State Chem. 66 (1987) 7–19.
[50] V. Peres, P. Fabry, F. Genet, J. Eur. Ceram. Soc. 13 (1994) 403–410.